Title

Comparison of accuracy and computational expense of radiation models in simulation of non-premixed turbulent jet flames

Journal

Combustion and Flame, 162(6)

ISSN

0010-2180

Authors

Pal, Gopalendu
Gupta, Ankur
Modest, Michael F
et al.

Publication Date

2015-06-01

DOI

10.1016/j.combustflame.2015.02.017

Peer reviewed

Combustion and Flame 162 (2015) 2487–2495

Contents lists available at ScienceDirect

Combustion and Flame

journal homepage: www.elsevier.com/locate/combustflame

Comparison of accuracy and computational expense of radiation models in simulation of non-premixed turbulent jet flames

Gopalendu Pal [a,*], Ankur Gupta [b], Michael F. Modest [c], Daniel C. Haworth [d]

[a] CD-Adapco, 21 Lafayette Street, Suite 100, Lebanon, NH 03766, USA
[b] COMSOL Inc., Burlington, MA 01803, USA
[c] School of Engineering, University of California, Merced, CA 95343, USA
[d] Mechanical and Nuclear Engineering Department, The Pennsylvania State University, University Park, PA 16802, USA

ARTICLE INFO

Article history:
Received 16 February 2015
Received in revised form 16 February 2015
Accepted 19 February 2015
Available online 17 March 2015

Keywords:
Nonpremixed turbulent flames
Radiative transfer equation
Spectral radiation properties
Turbulence–radiation interactions
Probability density function method

ABSTRACT

The accuracy and computational expense of various radiation models in the simulation of turbulent jet flames are compared. Both nonluminous and luminous methane–air nonpremixed turbulent jet flames are simulated using a comprehensive combustion solver. The combustion solver consists of a finite-volume/probability density function-based flow–chemistry solver interfaced with a high-accuracy spectral radiation solver. Flame simulations were performed using various *k*-distribution-based spectral models and radiative transfer equation (RTE) solvers, such as *P-1*, *P-3*, finite volume/discrete ordinates method (FVM/DOM), and line-by-line (LBL) accurate Photon Monte Carlo (PMC) methods, with and without consideration of turbulence–radiation interaction (TRI). Various spectral models and RTE solvers are observed to have strong effects on peak flame temperature, total radiant heat source and NO emission. The *P-1* method is found to be the computationally least expensive RTE solver and the FVM the most expensive for any spectral model. For optically thinner flames all radiation models yield excellent accuracy. For optically thicker flames the *P-3* and the FVM with advanced *k*-distribution methods predict radiation more accurately than the *P-1* method with any spectral model when compared to the benchmark LBL PMC. The LBL PMC yields exact results with sufficient number of samples and is found to be less expensive than the FVM (for all spectral models) and the *P-3* (for some spectral models) in statistically stationary combustion simulations. TRI is found to drop the peak temperature by close to 150 K for a luminous flame (optically thicker) and 25–100 K for a nonluminous flame (optically thinner).

1. Introduction

Thermal radiation plays an important role in multi-phase (gas + particulate phase) turbulent combustion systems. Until recently it was not possible to make high-accuracy predictions of radiative heat transfer rates in high-temperature combustion applications. The reasons for this deficiency are: (i) lack of high accuracy and efficient radiative transfer equation (RTE) solvers and (ii) lack of versatile, robust and computationally efficient models to predict radiation from nongray multi-phase media.

Because of the difficulties associated with radiation calculations, it has been common practice in turbulent flame simulations to invoke the optically-thin approximation, and/or to assume the medium to be gray, for both luminous [1] and nonluminous [2] flames. The optically-thin radiation model can result in substantial error due to its neglect of self-absorption, as has been shown by both numerical and experimental studies [3]. The gray medium assumption can also result in large errors as was shown by Li and Modest [4] and Wang et al. [5,6]. Nongray radiation modeling has begun to draw attention in combustion simulations [6,5]. Nongray radiation calculations in participating media can be most accurately performed using the line-by-line (LBL) approach, which, in order to resolve the spectrum, requires in excess of one million spectral solutions of the RTE, making such radiation calculations prohibitive. Models for nongray radiative properties include the weighted sum of gray gases (WSGG) [7], the spectral line-based weighted sum of gray gases (SLW) [8], and the full spectrum *k*-distribution (FSK) method [9]. The FSK method is an exact method for a homogeneous or correlated medium using a continuous *k*-distribution over the entire spectrum. Several advancements to the *k*-distribution method have been

* Corresponding author. Fax: +1 603 643 9994.
E-mail addresses: gopalendu@gmail.com (G. Pal), ankur.gupta@comsol.com (A. Gupta), mmodest@ucmerced.edu (M.F. Modest), dch12@engr.psu.edu (D.C. Haworth).

http://dx.doi.org/10.1016/j.combustflame.2015.02.017
0010-2180/

proposed to address the shortcomings of the basic FSK scheme in strongly inhomogeneous media based on the multi-scale (MS) [10] and the multi-group (MG) approaches [11], which may be summarized as: (1) the hybrid multi-scale multi-group FSK (MSMGFSK) method [12] for inhomogeneous gas mixtures, (2) the MSFSK method [13] for mixing of nongray soot with gas mixtures with/without gray wall emission, and (3) the narrow band-based hybrid MSMGFSK method [14] for inhomogeneous nongray gas–soot mixtures with/without wall emission. Recently, a portable spectral module has been developed by Pal et al. incorporating the LBL and all of the *k*-distribution methods with corresponding *k*-distribution databases to facilitate spectral radiation calculations [15].

Common methods for the solution of the RTE in turbulent combustion simulations are: (1) the spherical harmonics method (SHM), (2) the finite volume/discrete ordinates method (FVM/DOM), and (3) the photon Monte Carlo (PMC) method [16]. While the first two are deterministic in nature, the third is a statistical method. Statistical methods like the PMC can solve the most complicated problems with relative ease, but they are always subject to statistical error and require great computational power. Both the SHM and the FVM/DOM approximate the directional variation of the radiative intensity. However, the underlying approaches to represent the directional dependence of radiative intensity for SHM and FVM/DOM are quite different. The FVM/DOM employs a discrete representation of the directional variation with integrals over total solid angle 4π while the SHM captures the directional distribution of intensity by expressing it into a series of spherical harmonics. The FVM/DOM method is relatively simple to implement, but has several drawbacks, such as the fact that an iterative solution is required in the presence of scattering media or reflecting surfaces. In addition, its convergence is known to slow down for optically thick media where the directional discretization is required to be as fine as the spatial discretization to avoid the ray effects. The *P-1* method has so far been the most popular RTE solver within the SHM framework because of its simplicity, fairly good accuracy and its low requirement of computational time [4–6]. However, its accuracy is questionable in the presence of directionally inhomogeneous intensity distributions [16]. To achieve better accuracy, a number of higher-order *P-N*-approximations have been formulated [16]. Recently, Modest and Yang formulated a generic methodology that decomposes the RTE into $N(N+1)/2$ coupled second-order elliptic partial differential equations (PDE) for a given odd order *N*, allowing for variable properties and arbitrary three-dimensional geometries, including a set of generic boundary conditions [17].

Traditional turbulent combustion calculations treat radiation and turbulence as uncoupled processes using mean temperatures and concentrations to evaluate radiative properties and intensities [18]. Turbulence–radiation interaction (TRI) has been largely ignored to date due to its extreme complexity, even though its importance has been widely recognized [18]. Modest and coworkers [19] were the first to accurately model turbulent radiative emission within the context of the stochastic probability density function (PDF) method [20]. Typically the absorption coefficient–intensity correlation, i.e., "absorption TRI" was closed by invoking the optically thin fluctuation assumption (OTFA) [21]. Recently, a new approach, based on the photon Monte Carlo method for media represented by particle fields, has been developed by Wang and Modest [22], which evaluates absorption TRI exactly. Modest, Haworth and coworkers [18] used the composition PDF/Monte Carlo method to study radiative heat transfer in reactive flows.

The objective of this paper is to compare the effects of various spectral models for nongray multi-phase media, RTE solvers, and turbulence–radiation interactions in simulations of nonluminous and luminous methane–air turbulent jet flames. To the authors' knowledge, such detailed comparative study of radiation modeling in turbulent combustion simulation is absent from the literature. A high-accuracy hybrid flow–chemistry solver (finite volume flow solver + stochastic PDF chemistry solver) is interfaced with a spectral radiation solver, which is capable of performing combustion calculations for a three-dimensional unstructured mesh. The radiation module comprises four RTE solvers: *P-1*, *P-3* and FVM solvers implemented using the data structures of the finite-volume flow solver, and a stochastic PMC solver. The finite-volume-based radiation solvers are interfaced with a *k*-distribution-based spectral module and the stochastic PMC solver with a LBL module. The effects of various spectral models, RTE solvers and the consideration of TRI on flame radiant heat source, temperature, and NO emissions are discussed.

2. Numerical and physical models

2.1. Turbulent flow field

In this study a high-fidelity open source-code flow calculation software OpenFOAM [23] is employed as a finite-volume (FV) solver for Favre-averaged flow equations on an unstructured mesh. The equations include conservation of mass, momentum and enthalpy. A standard two equation k–ε model is employed as a turbulence model [24]. An iteratively implicit, segregated solution procedure solves the coupled system of governing PDEs for collocated cell-centered variables. Here statistically steady-state solutions are reached by time marching.

2.2. Composition PDF method

In composition PDF methods physical scalars, including temperature and species concentrations, are treated as independent random variables. The joint PDF is a function of spatial location, time and composition space. Once the joint PDF is obtained at a certain position $\underline{x}$ and time instant t, the mean value for any function, Q, of these scalars can be evaluated exactly as

$$\langle Q(\underline{x},t)\rangle = \int_{-\infty}^{\infty} Q(\underline{x},t) f(\underline{\psi};\underline{x},t)\,\mathrm{d}\underline{\psi} \tag{1}$$

where $\underline{\phi}(\underline{x},t)$ is the vector of physical scalars, $\underline{\psi}$ is the corresponding random variable vector, Q is a function of $\underline{\phi}$ only and f is the joint PDF, which represents the probability density of a compound event $\underline{\phi}=\underline{\psi}$. In practice the mass density PDF, $\mathcal{F}(\underline{\psi};\underline{\mathbf{x}},t)=\langle\rho(\underline{\mathbf{x}},t)\rangle f(\underline{\psi};\underline{\mathbf{x}},t)$, is more convenient and frequently used and its transport equation can be derived based on the conservation of scalars as [18]

$$\begin{aligned}\frac{\partial\mathcal{F}}{\partial t}+\frac{\partial}{\partial x_i}[\widetilde{u}_i\mathcal{F}]+\frac{\partial}{\partial\psi_\alpha}[S_{\alpha,\mathrm{reac}}(\underline{\psi})\mathcal{F}] = &-\frac{\partial}{\partial x_i}\left[\left\langle u_i''\mid\underline{\psi}\right\rangle\mathcal{F}\right]\\ &+\frac{\partial}{\partial\psi_\alpha}\left[\left\langle\frac{1}{\rho}\frac{\partial J_i^\alpha}{\partial x_i}\mid\underline{\psi}\right\rangle\mathcal{F}\right]\\ &-\frac{\partial}{\partial\psi_s}[\langle S_{\mathrm{rad}}|\underline{\psi}\rangle)\mathcal{F}]\end{aligned} \tag{2}$$

where i and α are summation indices in physical space and composition space, respectively, and $\langle A|B\rangle$ is the conditional mean of event A, given that event B occurs. Variables with tildes and double primes are Favre means of the variables and fluctuations about them. u is the velocity vector, J is the flux due to molecular diffusion and S source term due to chemical reaction and radiation. Terms appearing on the left-hand side of Eq. (2) can be accounted for exactly. The first two terms are the rate of change and the advection of the PDF in the Favre-averaged mean flow. The third term is the transport of the PDF in composition space due to

chemical reactions including turbulence–chemistry interactions. Terms on the right-hand side must be modeled. The first two terms represent the transport in physical space due to turbulent convection and transport in composition space due to molecular mixing, respectively, and are commonly modeled using the gradient-diffusion hypothesis and a pair-exchange mixing model (details can be found in Haworth [18]). The third term on the right-hand side of Eq. (2) is the transport of the composition PDF due to radiative transfer. The radiative source is the difference between the energy gain due to absorption of incident radiation and energy loss due to local emission as

$$S_{\text{rad}} = -\nabla \cdot \underline{q}^R = \int_0^\infty \kappa_\eta (G_\eta - 4\pi I_{b\eta}) \mathrm{d}\eta, \quad G_\eta = \int_{4\pi} I_\eta \mathrm{d}\Omega \tag{3}$$

where I_η is the spectral radiative intensity, κ_η is the local spectral absorption coefficient, $I_{b\eta}$ is the local spectral blackbody intensity, Ω is the solid angle and G_η is the incident radiative intensity integrated over the entire solid angle of 4π. Both κ_η and $I_{b\eta}$ are functions of local composition variables only and, therefore, can be evaluated exactly. In contrast, G_η depends on the properties at every point in the domain, and the one-point PDF employed here is not sufficient to close this term and, hence, it must be modeled.

The PDF transport equation Eq. (2) is usually solved by particle Monte Carlo methods, in which the PDF is discretized into a sufficiently large number of delta functions (particles) carrying their own scalars. The particles are traced and scalars carried are mixed over time according to the Lagrangian form of Eq. (2) [20]. The composition PDF method is not self-sustained, requiring the solution of the mean flow field to supply mean velocity and turbulence quantities to be used in the stochastic differential equations. The composition PDF code [25] is connected to OpenFOAM and is employed to solve for scalars (temperature and species concentrations). Consistency is maintained between the mean particle mass and finite-volume fluid mass at the finite-volume element level [25]. An augmented reduced chemical mechanism (ARM2) for methane–air combustion, which involves 19 species and 15 reactions (including NO chemistry), is incorporated into the PDF-based chemistry calculations [27].

2.3. Radiation model

2.3.1. k-Distribution method

The *k*-distribution method reorders the rapidly oscillating absorption coefficients across the spectrum into a well-behaved smooth monotonically increasing function *vs* a cumulative distribution function *g*, which acts as a nondimensional wavenumber. The tedious integration over wavenumber space can then be replaced by integration over *g*-space using a small number of quadrature points. The radiative transfer equation (RTE) for an emitting-absorbing-scattering medium on a spectral basis can be written as [16]

$$\frac{\mathrm{d}I_\eta}{\mathrm{d}s} = \kappa_\eta(\underline{\phi}) I_{b\eta} - \left(\kappa_\eta(\underline{\phi}) + \sigma_{s\eta}(\underline{\phi})\right) I_\eta + \frac{\sigma_{s\eta}(\underline{\phi})}{4\pi} \int_{4\pi} I_\eta(\hat{s}') \Phi_\eta(\underline{\phi})(\hat{s}, \hat{s}') d\Omega' \tag{4}$$

where $\sigma_{s\eta}$ is the spectral scattering coefficient. The vector $\underline{\phi}$ contains state variables that affect κ_η and $\sigma_{s\eta}$, which include temperature T, total pressure P, and gas mole fractions $\underline{x}$: $\underline{\phi} = (T, P, \underline{x})$. $\hat{s}$ is a unit direction vector, and Φ_η is the spectral scattering phase function. In the most advanced FSK method, i.e., the MSMGFSK method [14], the mixture's spectral absorption coefficient κ_η is first separated into contributions from N component species, and then the spectral locations of the n-th gas absorption coefficient are sorted into M exclusive spectral groups according to their temperature dependence, i.e.,

$$\kappa_\eta = \sum_{n=1}^{N} \sum_{m=1}^{M_n} \kappa_{nm\eta}, \quad I_\eta = \sum_{n=1}^{N} \sum_{m=1}^{M_n} I_{nm\eta} \tag{5}$$

The radiative intensity I_η is also broken up accordingly. The RTE, Eq. (4), is then transformed into $\sum_{n=1}^{N} M_n$ component RTE's, one for each group of each species scale (assuming gray scattering):

$$\frac{\mathrm{d}I_{nm\eta}}{ds} = \kappa_{nm\eta} I_{b\eta} - (\kappa_\eta + \sigma_s) I_{nm\eta} + \frac{\sigma_s}{4\pi} \int_{4\pi} I_{nm\eta}(\hat{s}') \Phi(\hat{s}, \hat{s}') d\Omega', \quad \text{for } n = 1, \ldots, N;\ m = 1, \ldots, M_n \tag{6}$$

Note that the intensity $I_{nm\eta}$ is due to emission by the m-th group of the n-th scale (the nm-th group) but subject to absorption by all groups of the other scales and its own group. The FSK reordering is done by multiplying Eq. (6) by a Dirac-delta function, followed by integration over the entire spectrum [14] as

$$\frac{\mathrm{d}I_{nmg}}{\mathrm{d}s} = k_{nmg} a_{nmg} I_b - (\lambda_{nmg} + \sigma_s) I_{nmg} + \frac{\sigma_s}{4\pi} \int_{4\pi} I_{nmg}(\hat{s}') \Phi(\hat{s}, \hat{s}') d\Omega', \quad \text{for } n = 1, \ldots, N;\ m = 1, \ldots, M_n \tag{7}$$

where a_{nmg} is a nongray stretching factor and λ_{nmg} is the overlap parameter for the m-th group of the n-th scale (details can be obtained from Pal and Modest [14]). Employing the MSMGFSK method, the radiative heat source, Eq. (3), becomes

$$S_{\text{rad}} = \sum_n \sum_m \int_0^1 (\lambda_{nmg} G_{nmg} - 4\pi k_{nmg} a_{nmg} I_b) \mathrm{d}g \tag{8}$$

From the MSMGFSK method a single-group MSFSK method (with N scales) can also be obtained by letting $M_n = 1$ and the basic single-group-single-scale FSK method is retrieved by setting $M_n = N = 1$ (and $\lambda_g = k_g$).

2.3.2. RTE solver

The *k*-distribution methods are designed to work with any RTE solution method. Here the spherical harmonic methods, i.e. the *P-1* and *P-3* approximations, and the FVM method are employed. Different RTE solvers require different numbers of equations – only one elliptical PDE needs to be solved for the *P-1* approximation, whereas, based on the formulation of Modest and Yang [17], 6 coupled second-order elliptic PDEs are required for the *P-3* approximation. In the FVM method the number of first order PDEs to be solved depends on the angular discretization. In this study various angular discretizations are considered but results with 6×2 and 16×4 angular discretizations ($\theta \times \phi$) only are presented. For brevity of mathematical formulations only the *P-1* approximation with *k*-distribution spectral models are shown here. Details of the FVM method can be obtained from Modest [16] and the *P-3* approximation with generic boundary conditions can be found in Modest and Yang [17]. Application of the *k*-distribution methods to the FVM and *P-3* equations is similar to the *P-1* equation. With the *P-1* approximation and the MSMGFSK method in conjunction with the assumption of isotropic scattering, the reordered RTE, Eq. (7), becomes

$$\nabla \cdot \left(\frac{1}{\lambda_{nmg} + \sigma_s} \nabla G_{nmg} \right) - 3\lambda_{nmg} G_{nmg} + 12\pi k_{nmg} a_{nmg} I_b = 0 \tag{9}$$

The boundary condition is derived by placing all wall emission into one of the species scales (e.g., the n-th scale), usually the single-group soot scale ($M = 1$) because of its continuous nature, and can be written as

$$-\frac{2-\epsilon}{\epsilon} \frac{2}{3(\lambda_{ng} + \sigma_s)} \hat{\mathbf{n}} \cdot \nabla G_{ng} + G_{ng} = 4\pi \lambda_{ng} a_{wg} I_{bw} \tag{10}$$

where $\hat{\mathbf{n}}$ is the outward unit surface normal at a boundary, ϵ is the surface emittance, and a_{wg} and I_{bw} are evaluated at the surface

temperature T_w. For all other scales (without wall emission) the boundary conditions are the same but with zero right hand side.

The *P-1*, *P-3* and FVM RTE solvers have been implemented using the data structures and solver libraries of the open source-code flow software OpenFOAM [23] for any generic unstructured grid system. The *P-1*, *P-3* and FVM RTE solvers are interfaced with the spectral module [15] via the PDF module [25]. The PMC module (with its own LBL databases) developed by Wang [24] is also interfaced with the hybrid finite-volume/PDF software as a part of the comprehensive combustion solver package. A schematic of the interface of various solver modules and the data flow are shown in Fig. 1. This interface allows data passing between the C++-based FV solvers (flow and FV RTE solvers in OpenFOAM) and the FORTRAN90-based PDF, PMC solvers and spectral module (SRCS).

2.3.3. Turbulence–radiation interactions

For Reynolds-averaged simulations Eq. (3) is averaged to yield

$$\langle S_{\text{radiation}}\rangle = \int_0^\infty \left(\langle \kappa_\eta G_\eta\rangle - 4\pi\langle \kappa_\eta I_{b\eta}\rangle\right) d\eta \tag{11}$$

In general,

$$\begin{aligned}
&\langle I_{b\eta}\rangle \neq I_{b\eta}(\langle T\rangle),\\
&\langle \kappa_\eta I_{b\eta}\rangle \neq \kappa_\eta\left(\langle \underline{\phi}\rangle\right) I_{b\eta}(\langle T\rangle),\\
&\langle \kappa_\eta G_\eta\rangle \neq \kappa_\eta\left(\langle \underline{\phi}\rangle\right)\langle G_\eta\rangle
\end{aligned} \tag{12}$$

The terms in Eq. (12) are called temperature, emission and absorption TRI correlations, respectively. Both κ_η and $I_{b\eta}$ are functions of local composition variables only and, therefore, emission TRI can be evaluated exactly using the one-point composition PDF method. On the other hand, G_η depends on the properties at every point in the domain, and the one-point PDF employed here is not sufficient to close this term. Only when using the discrete particle PMC scheme developed by Wang and Modest [22] absorption TRI can be evaluated exactly, whereas for the case of a finite-volume-based RTE solvers absorption TRI needs to be modeled through the OTFA [21], i.e., for optically thin eddies

$$\langle \kappa_\eta G_\eta\rangle \approx \langle \kappa_\eta\rangle\langle G_\eta\rangle \tag{13}$$

3. Flame simulations

3.1. Nonluminous flame

3.1.1. Flame D

Flame D measured by Barlow and Frank at Sandia National Laboratories [28] is employed to validate the proposed solver.

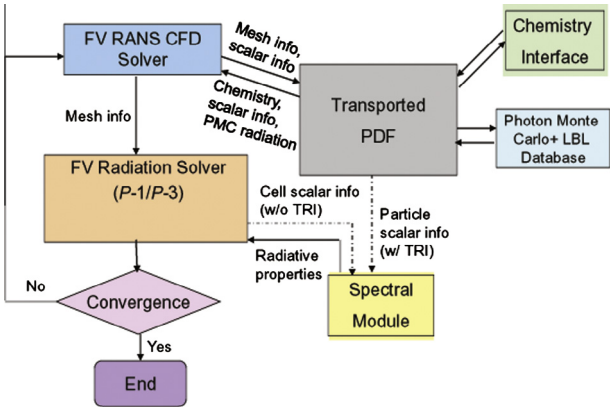

Fig. 1. Schematic of interfacing of the FV spectral radiation solver with the flow-chemistry solver.

The experimental setup of Flame D may be summarized as follows: the fuel jet (diameter $d_j = 7.2$ mm) with high velocity ($u_j = 49.6$ m/s) is surrounded by an annular pilot flow ($d_p = 18.4$ mm, $u_p = 11.4$ m/s) consisting of the products of a burnt methane/air mixture with an equivalence ratio of 0.77, and a slow outer air coflow ($u_c = 0.9$ m/s); the fuel is a mixture of air and methane with a volume ratio of 3:1. In the present study a wedge-like 3-D grid system consisting of 3300 cells is employed to simulate 2-D axisymmetric flames by applying periodic boundary conditions on the sides. The wedge angle is 10° and its dimensions in the x- and y-directions are $20d_j$ and $100d_j$, respectively. It has been found that around 30 PDF stochastic particles per cell on average are sufficient to resolve turbulence fluctuations in the considered flames. Therefore, roughly 80,000 particles are used to populate the entire computational domain. For the radiation simulation, the inlet and the side boundary are treated as cold and black, while the exit is treated to be diffusely reflective. In coupled simulation using the LBL PMC RTE solver a total of 80,000 photon bundles are traced in each time step and the feedback is time blended over 1000 iterations. Details of this scheme can be found in Wang et al. [24]. For coupled simulation using FV RTE solvers, full radiation feedback is given in each time step. If a time-accurate solution is desired, the radiative feedback has to be calculated correctly for each time step (rather than time blending over a number of iterations). In time-accurate coupled simulations the LBL PMC requires a much larger number of photon bundles (>50 million) to be traced per time step for statistical convergence [26] whereas the radiation feedback by FV RTE solvers are time-accurate by its nature. Hence, for time-accurate cases LBL PMC becomes computationally prohibitive while computational expense remains unchanged for FV RTE solvers between statistically stationary and time-accurate coupled simulations. In the following flame simulations a time step of 1 μs has been used during the initial stages of calculations, and increased to 50 μs during later stages when calculations are stabilized.

In traditional finite-volume methods the residual error diminishes to zero with sufficient number of iterations, and can be used as a criterion of convergence. However, the residual error in hybrid finite-volume/Monte Carlo methods never diminishes to zero due to statistical scatter. Therefore, it is impossible to use residual error as a criterion of convergence. The emission-averaged temperature (as employed by Wang [24]) is used here to monitor the convergence.

The effects of radiation and TRI are summarized in Table 1. It can be seen from Table 1 that consideration of radiation and TRI cools down the flame. With various RTE solvers and spectral models for Flame D there is a temperature drop between 31 and 44 K when radiation is considered without TRI and 54–65 K with TRI. It was observed for the FVM that at least 16×4 angular discretization is needed to achieve convergence in terms of angular discretization without any unphysical results (hot spots) in the colder part of the computational domain. Hence, results for only the FVM (16×4) case is shown and the results for coarser angular discretization are omitted. Since Flame D is an optically thin flame, all RTE solvers and spectral models yield similar results. Hence for such a case the simple *P-1* method with a gray spectral model will be sufficient to achieve good accuracy with less computational time in radiation calculations. It is also observed that the consideration of TRI increases radiative heat loss from Flame D by 26–27%.

The temperature drops have significant impact on NO generation as can be seen in Table 1 for Flame D. When radiation is considered without TRI, NO production is reduced approximately by a factor of 2 and with TRI by 2.2. Simulation results of Flame D are compared with experimental measurements. Radial profiles of

Table 1
Effect of radiation models and TRI in simulation of nonluminous Flame D.

Configuration	Radiation	RTE solver	Spectral model	TRI	Peak mean T (K)	NO emission index (g_{NO}/kg_{fuel})	Net $\nabla \cdot q_R$ (kW)	% △TRI
Flame D	Off				2015	1.74		
	On	PMC	LBL	No	1984	0.93	0.52	
				Yes	1961	0.81	0.66	27
		Optically thin		No	1971	0.82	0.71	
				Yes	1950	0.74	0.88	24
		P-1	Gray	No	1976	0.88	0.53	
				Yes	1953	0.80	0.68	28
			FSK	No	1977	0.88	0.53	
				Yes	1958	0.80	0.67	26
		P-3	FSK	Yes	1959	0.80	0.67	
		FVM (16 × 4)	FSK	Yes	1959	0.80	0.67	

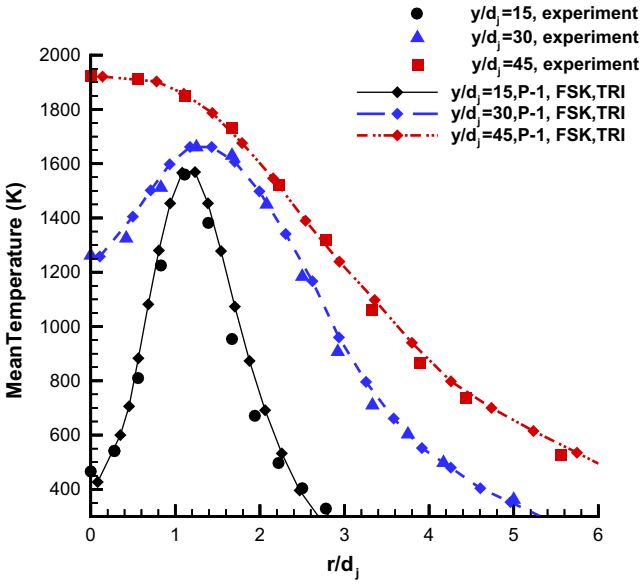

Fig. 2. Radial profiles of mean temperature at various axial locations of Flame D.

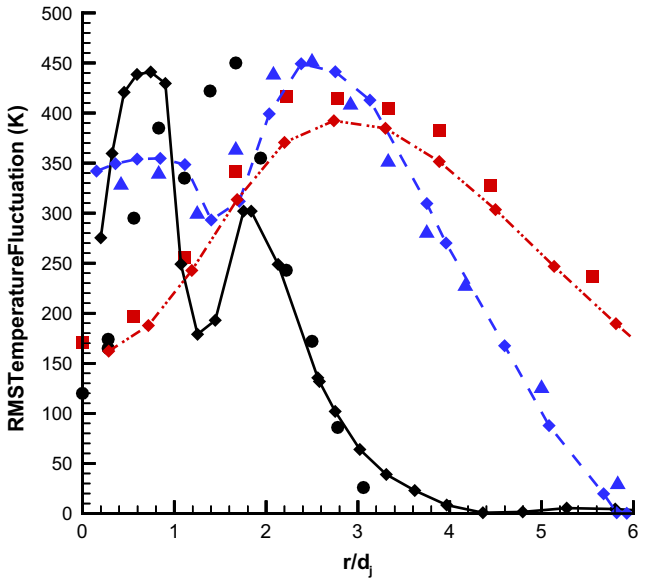

Fig. 3. Radial profiles of RMS temperature fluctuations at various axial locations of Flame D (same legends as in Fig. 2).

mean and RMS values of temperature and NO mass fraction at various axial locations (z/d_j) are shown in Figs. 2–5. An excellent match is observed between the experimental measurements and simulation results when radiation with TRI is considered. Calculations without radiation, shown only for the NO mass fraction, overpredict values by close to an order of magnitude and, thus, can lead to erroneous prediction of pollution even for flames with such small radiant fraction.

3.1.2. Flame 4×D

Besides Flame D, one additional artificial nonluminous flame (termed Flame 4×D) is derived from it by quadrupling the jet diameter to increase the flame optical thickness while keeping the Reynolds number constant (i.e., decreasing velocity). It can be seen from Table 2 that for this optically thicker flame, Flame 4×D, radiation models play an important role. When radiation is considered without TRI (excluding the optically thin radiation model) the flame temperature drops by more than 100 K, and when TRI is considered by additional 100 K. For all radiation models, consideration of TRI enhances heat transfer by at least 38% and up to 43%. Optically thin radiation, which has been traditionally used as a simplified radiation model in many flame simulations, is seen to (in combination with TRI) severely overpredict the radiative heat loss and drop the peak flame temperature by 300 K and NO emission index by two orders of magnitude. Simplification of radiation model by optically thin assumption yields erroneous

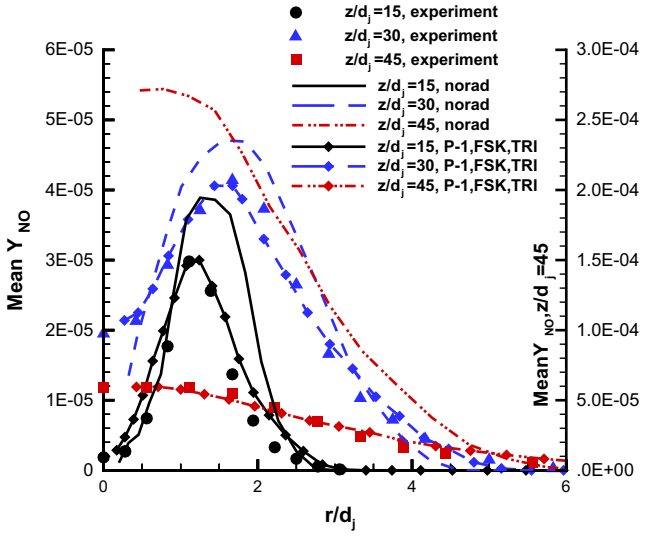

Fig. 4. Radial profiles of mean NO mass fraction at various axial locations of Flame D.

results for such flames. When various spectral models are compared, keeping the RTE solver and TRI mode fixed, e.g., *P-1* with full TRI, we observe that the net radiative heat source decreases by

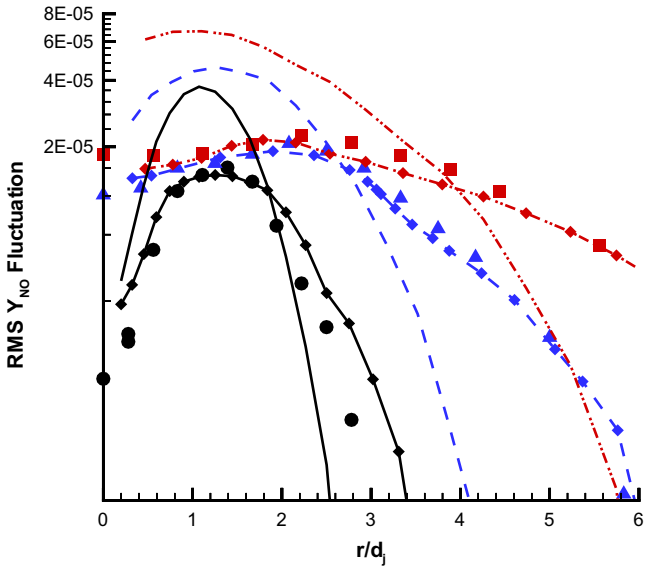

Fig. 5. Radial profiles of RMS fluctuations of NO mass fraction at various axial locations of Flame D (same legends as Fig. 4).

close to 2% as we go from FSK to MSFSK (with 2 scales – CO_2 and H_2O as one combined scale and CH_4 as the other scale). Since results remains virtually the same from MSFSK to MSMGFSK (CO_2, H_2O, and CH_4 each as separate scales with CO_2 and H_2O having 2 groups each), it has not been included in Table 2. Thus, one may consider the MSFSK spectral model to be the optimum spectral model for this problem, considering a compromise between accuracy and computational time. Since various spectral models predict radiative heat source terms differently, which directly affect the temperature distribution, a profound effect is observed on NO emission indices as can be seen in Table 2. When radiation is considered without TRI (excluding optically thin model) the NO emission index drops approximately by a factor of 6, and when TRI is considered, by another factor of 8. NO generation is observed to increase as one goes from FSK to MSFSK (for the *P-1* and FVM (16×4) RTE solvers with TRI) approximately by a factor of 1.4 whereas for the *P-3* RTE solver, it decreases by a factor of 1.2. For any given RTE solver, the MSFSK model predicts combustion parameters slightly more accurately (compared to the benchmark LBL PMC) than FSK, although FSK is found to yield overall excellent accuracy.

When results from various RTE solvers are compared (from Table 2), keeping the spectral model and TRI mode the same, e.g., FSK with full TRI, we see that the *P-1* and the FVM (16×4) overpredict the net radiative heat source by close to 7.2% and 1.2% respectively compared to the LBL PMC while the *P-3* underpredicts the net radiative heat source by 3.5%. For this flame the FVM (16×4) predicts the NO emission index exactly whereas *P-1* slightly underpredicts and *P-3* slightly overpredicts this parameter. For Flame 4×D FVM (16×4) RTE solver with the MSFSK spectral model and TRI produces results of highest accuracy, the *P-1* is the least accurate solver while the *P-3* is negligibly less accurate compared to the FVM (16×4) solver.

3.2. Luminous flame – Flame 4×D+Soot

Radiation and TRI effects are closely related to the optical thickness of flames and turbulent eddies. Such effects tend to be more prominent in sooting flames, since the presence of soot may greatly increase the optical thickness. The third flame investigated is an artificial luminous flame (termed Flame 4×D+Soot) derived by incorporating artificial soot calculations based on an algebraic state relationship in simulation of Flame 4×D. The empirical state relationship (modified from the state relationship used by Mazumder [29]) used here for the evaluation of soot volume fractions is given by

$$f_v = 10^{4T/3000-2/3} \times \begin{cases} 10^{-7}\Phi^{1.44}, & 0.5 \leqslant \Phi < 1.0 \\ 10^{-7}\Phi^{4.73}, & 1.0 \leqslant \Phi < 1.33 \\ 4.19 \times 10^{-5}\Phi^{-5}, & 1.33 \leqslant \Phi < 1.6 \end{cases} \quad (14)$$

where Φ is the equivalence ratio defined as the ratio of the fuel-to-oxidizer ratio to the stoichiometric fuel-to-oxidizer ratio. Typical peak soot volume fraction predicted by this method for Flame 4×D+Soot is around 6 ppm.

Simulation results of Flame 4×D+Soot are presented in Table 3. It is observed that, in presence of soot, radiation plays an extremely important role. Radiation without TRI (excluding optically thin model) drops the flame temperature by more than 150 K, and when TRI is considered by an additional 150 K. Consideration of TRI enhances heat transfer by at least 62% and up to 66%. During comparison of various spectral models for the *P-1* solver with TRI, similar to the Flame 4×D, we observe that the net radiative heat source increases by close to 5% as we go from FSK to MSFSK. For radiation without TRI (excluding optically thin model) the NO emission index drops approximately by a factor of 25, and when TRI is considered, by another factor of 6–8. NO generation is observed to increase as one goes from FSK to MSFSK (for the *P-1* RTE solver) approximately by a factor of 2.5. For the *P-1* RTE solver the FSK method (with TRI) is slightly more accurate than the

Table 2
Effect of radiation models and TRI in simulation of nonluminous Flame 4×D.

Configuration	Radiation	RTE solver	Spectral model	TRI	Peak mean T (K)	NO emission index (g_{NO}/kg_{fuel})]	Net $\nabla \cdot q_R$ (kW)	% △TRI
Flame 4×D	Off				2011	7.50		
	On	PMC	LBL	No	1901	1.20	11.8	
				Yes	1799	0.15	16.6	41
		Optically thin		No	1801	0.17	16.5	
				Yes	1699	0.05	23.4	41
		P-1	FSK	No	1864	0.81	12.6	
				Yes	1766	0.08	17.8	41
			MSFSK	No	1884	0.90	12.1	
				Yes	1790	0.11	16.8	38
		P-3	FSK	No	1911	1.30	11.3	
				Yes	1819	0.24	16.0	41
			MSFSK	No	1909	1.30	11.4	
				Yes	1814	0.20	16.1	41
		FVM (16×4)	FSK	No	1889	1.05	11.9	
				Yes	1791	0.11	16.8	41
			MSFSK	No	1892	1.08	11.7	
				Yes	1794	0.15	16.7	43

Table 3
Effect of radiation models and TRI in simulation of luminous Flame 4×D+Soot.

Configuration	Radiation	RTE solver	Spectral model	TRI	Peak mean T (K)	NO emission index (g_{NO}/kg_{fuel})	Net $\nabla \cdot q_R$ (kW)	% △TRI
Flame 4×D+Soot	Off				2011	7.50		
	On	PMC	LBL	No	1854	0.30	18.5	
				Yes	1701	0.05	30.6	65
		Optically thin		No	1701	0.06	30.8	
				Yes	1588	0.001	50.7	65
		P-1	FSK	No	1821	0.21	21.6	
				Yes	1690	0.03	35.1	63
			MSFSK	No	1813	0.19	22.9	
				Yes	1688	0.08	37.2	62
		P-3	FSK	No	1860	0.36	17.6	
				Yes	1704	0.05	29.1	65
			MSFSK	No	1858	0.35	18.0	
				Yes	1702	0.05	29.6	64
		FVM (16 × 4)	FSK	No	1848	0.32	19.6	
				Yes	1693	0.04	32.1	63
			MSFSK	No	1850	0.34	18.7	
				Yes	1699	0.05	31.0	66

MSFSK method while for the other FV RTE solvers the MSFSK method yields better accuracy than the FSK.

When results from various RTE solvers are compared (from Table 3), as done for the Flame 4×D, we see that the *P-1* and the FVM (16 × 4) overpredict the net radiative heat source by approximately 15% and 5% respectively compared to the LBL PMC while the *P-3* underpredicts the net radiative heat source by approximately 5%. For Flame 4×D+Soot both the *P-3* and the FVM (16 × 4) RTE solvers with the MSFSK spectral model and TRI produce excellent accurate results.

3.3. Computational time comparison

All simulations were performed on Triton, a PC Cluster run by the High Performance Computing Group of the University of California, San Diego. The cluster consists of 256 nodes, each of which has four 3.0 GHz Intel Nehalem E5530 dual-core processors. The newly developed combustion solver with FV spectral radiation solver is completely domain-decomposable and, hence, can be efficiently run in parallel. The FV RTE solvers are designed to store the values of intensity/incident radiation from the previous time step solution and these values are used as the initial guess by the RTE solver during the current time step. Since these values change only by a small amount in a time marching scheme, hence, the previous time step solution can provide an excellent initial guess. This facilitates fast convergence in the RTE solution. In this paper coupled simulations were performed in parallel using 16 processors (2 nodes with 8 processors in each). Simple domain decomposition into cell blocks along the axial direction was used throughout the study. Table 4 shows the averaged CPU time spent in one time step by various components of calculations, such as the spectral model, RTE solver and flow+chemistry solver during the simulation of Flame 4×D+Soot. It is seen from Table 4 that a parallel efficiency (ϵ) of approximately 80% is obtained for all calculations although no special effort was invested to enhance the parallel efficiency. It is also apparent from Table 4 that the computational time increases as one goes from the basic FSK to the more advanced MSFSK and MSMGFSK spectral models (for a given RTE solver, e.g, *P-1*) both in property calculations ($t_{\text{rad prop}}$) and RTE solutions (t_{RTE}), because a larger number of RTEs needs to be solved with more advanced k-distribution methods. The *P-1* RTE solver is the least expensive RTE solver with all of the basic-to-advanced spectral models, while the FVM (16 × 4) is found to be the most expensive RTE solver for any given spectral model with accuracy close-to the *P-3* approximation. Computational time for the FVM (6 × 2) method is presented in Table 4 to compare with the *P-3* method since the FVM (6 × 2) solves 12 first order PDEs which is comparable to the *P-3* which solves 6 coupled second order PDEs. The *P-3* method is found to be faster and very accurate compared to the FVM (6 × 2) which is not only slower but less accurate due to coarse angular discretization. Although the *P-3* method with the most advanced MSMGFSK model yields extremely good accuracy (when compared to the exact LBL PMC), its computational expense per time step is much higher than the LBL PMC. Thus, when an extremely high accuracy is desired for a statistically stationary simulation, a LBL PMC RTE solver can rather be used to achieve an exact solution in less computational time than any deterministic radiation solver with advanced spectral models [24].

3.3.1. Frozen field study

Since radiation and combustion are fully coupled in the above simulations, different radiation treatments result in different feedback of enthalpy change and temperature distributions, which further yield different chemical reaction rates and gas species concentrations. Hence, a frozen field study is carried out in which a particle field is extracted from the above fully coupled full-TRI simulations after statistical convergence has been achieved. This study isolates the effects of various spectral models with a fixed RTE solver (*P-1*) with full TRI and the results are included in Table 5. These simulations were carried out in parallel using 16 processors. For Flame 4×D Table 5 indicates that the basic FSK method underpredicts the net heat loss by 4% while both the MSFSK and MSMGFSK (2 and 4 groups) yield excellent accuracy with differences limited to 1%. For Flame 4×D+Soot soot radiation dominates over gas radiation. Hence, the basic FSK spectral model yields excellent accuracy compared to LBL calculations. The accuracy in the prediction of total radiative heat loss increases only negligibly from FSK (≈1.5% inaccuracy) to more advanced k-distribution models (<1.0% inaccuracy).

Similar frozen field study was carried out isolating the effects of RTE solvers for the LBL spectral model. For statistical convergence a total of 80 million rays were used in the LBL PMC solver as outlined by Wang [26]. These simulations were performed in parallel using 64 processors. Results show that the RTE solver has a stronger effect on net radiation heat transfer for optically thicker flames specially when soot is present (see Table 6). For Flame 4×D the *P-1* RTE solver incurs 9% inaccuracy compared to the exact solution obtained by the LBL PMC, whereas the *P-3* predicts the net radiative heat loss to within 2% inaccuracy. For Flame 4×D+Soot the *P-1* solver overpredicts the heat source by 15% lowering the flame temperature significantly compared to the LBL PMC, whereas *P-3* predicts the net radiative heat loss within 5% inaccuracy. This

Table 4
Comparison of CPU time and parallel efficiency.

RTE solver	Spectral model	N_P	t_{prop} (s)	t_{RTE} (s)	$t_{rad} = t_{prop} + t_{RTE}$ (s)	$t_{total} = t_{flow} + t_{chem} + t_{prop} + t_{RTE}$ (s)	ϵ
P-1	FSK	1	0.32	0.10	0.42	73.14	1.00
		16	0.02	0.007	0.027	5.64	0.81
	MSFSK	1	0.64	0.16	0.80	73.53	1.00
		16	0.04	0.01	0.05	5.74	0.80
	MSMGFSK	1	1.60	0.41	2.01	74.73	1.00
		16	0.10	0.03	0.13	5.91	0.80
P-3	FSK	1	0.32	1.05	1.37	74.09	1.00
		16	0.02	0.07	0.09	5.78	0.80
	MSFSK	1	0.64	2.0	2.64	75.36	1.00
		16	0.04	0.14	0.18	5.88	0.80
	MSMGFSK	1	1.60	5.21	6.81	79.53	1.00
		16	0.10	0.36	0.46	6.26	0.79
FVM (6×2)	FSK	1	0.32	1.20	1.52	74.27	1.00
		16	0.02	0.08	0.10	5.75	0.81
	MSFSK	1	0.64	2.36	3.00	75.70	1.00
		16	0.04	0.16	0.20	5.91	0.80
	MSMGFSK	1	1.60	5.88	7.48	80.31	1.00
		16	0.10	0.39	0.49	6.27	0.80
FVM (16×4)	FSK	1	0.32	6.71	7.03	79.71	1.00
		16	0.02	0.44	0.46	6.31	0.79
	MSFSK	1	0.64	13.39	14.03	86.75	1.00
		16	0.04	0.86	0.90	6.86	0.79
	MSMGFSK	1	1.60	31.55	33.15	105.77	1.00
		16	0.10	2.63	2.73	8.48	0.78
PMC	LBL	1			3.20	75.92	1.00
		16			0.26	5.95	0.79

Table 5
Frozen-field studies on the influence of variations in the spectral model for the *P-1* RTE solver (computation using 16 processors).

Configuration	Spectral models	Net $\nabla \cdot q_R$ (kW)	% $\triangle(\nabla \cdot q_R)$	Time (s)
Flame 4×D	LBL	16.99		3.52×10^4
	FSK	16.29	−4.12	0.06
	MSFSK	17.18	1.12	0.09
	MSMGFSK (2 Group)	17.13	0.82	0.24
	MSMGFSK (4 Group)	17.13	0.82	0.53
Flame 4×D+Soot	LBL	36.3		3.52×10^4
	FSK	35.7	−1.65	0.06
	MSFSK	36.6	0.82	0.13
	MSMGFSK (2 Group)	36.5	0.55	0.33
	MSMGFSK (4 Group)	36.5	0.55	0.58

Table 6
Frozen-field studies on the influence of variations in the RTE solver for the LBL spectral model (computation using 64 processors).

Configuration	RTE solvers	Net $\nabla \cdot q_R$ (kW)	% $\triangle(\nabla \cdot q_R)$	Time (s)
Flame 4×D	PMC	15.61		61.72
	P-1	16.99	8.84	8.79×10^3
	P-3	15.92	1.98	8.80×10^4
	FVM (6×2)	14.18	−9.16	1.05×10^5
	FVM (16×4)	15.06	−3.52	5.71×10^5
Flame 4×D+Soot	PMC	31.6		39.8
	P-1	36.3	14.87	8.79×10^3
	P-3	33.2	5.06	8.80×10^4
	FVM (6×2)	26.1	−17.4	1.05×10^5
	FVM (16×4)	29.89	−5.41	5.71×10^5

implies that the presence of soot radiation lowers the accuracy of the *P-N* method. The presence of an optically thick layer of soot within the optically thinner gas mixture increases the inhomogeneity in intensity distribution and, hence, the *P-N* method starts performing poorly with overprediction of the local radiative heat source. As seen from Table 6, the FVM (6×2) and FVM (16×4) underpredict the net radiative heat loss by 9% and 4% respectively for Flame 4×D and by 17% and 5% respectively for Flame 4×D+Soot. For the flames studied in this paper *P-3* solver is found to be the most accurate deterministic RTE solver. Comparison of Tables 5 and 6 for *P-1* RTE solver shows that *P-1*+FSK yields slightly better accuracy than *P-1*+LBL. This may possibly be caused by compensating errors in FSK method.

Tables 5 and 6 also compare the computational cost for radiation calculations for a frozen field. The primary difference of this time data (for uncoupled simulation on frozen field) with the previous time data (for coupled simulation as shown in Table 4) is that here the *P-1* and *P-3* RTE solvers use arbitrary value (equals to zero for all the cases) as the initial guess rather than the solution from the previous time step which serves as an excellent initial guess. Thus, the *P-1* and *P-3* RTE solvers take more number of iterations and, hence, more time to converge. When time data are compared between Tables 4 and 5, it is observed that computational cost increases by twice if arbitrary initial guess is used. This justifies the storage of solution from the previous time step for the *P-1* and *P-3* RTE solvers. It is also apparent from Table 5 that the *k*-distribution methods reduce the computational cost by a factor of $\sim 7 \times 10^4$–6×10^5 compared to the LBL calculations. Table 6 shows the time comparison among various RTE solvers with the LBL model in frozen field calculation. The PMC achieves LBL accuracy with relatively few photon bundles since the method inherently uses the most important wavenumbers to find its own *k*-distribution, and is observed to be the least expensive. The FV RTE solvers require from several hours to few days to obtain solution for a given flow field in a LBL manner. The trend of computational requirement among various FV RTE solvers is same as in Table 4.

4. Conclusion

Simulation of nonpremixed methane–air turbulent jet flames and comparison of various radiation models are performed in this paper. A combustion solver equipped with finite-volume/PDF flow–chemistry modules as well as spectral radiation modules is used in this study. Results from different finite-volume RTE solvers with *k*-distribution-based spectral models are compared with the benchmark LBL PMC calculations. For optically thin flames all radiation models are found to perform equally well and, thus, the basic *P-1*+gray model will produce excellent accuracy with less computational time. For optically thicker flames differences in results among various radiation models are observed. RTE solvers are found to have a larger impact on radiation calculations than the spectral models. The *P-3* RTE solver with the MSFSK spectral model is capable of yielding close-to LBL PMC accuracy for the flames studied with less computational cost than the corresponding FVM and PMC methods. For a statistically stationary simulation the LBL PMC yields exact answer with computational time close to the *P-3* and FVM (16×4), although application of the LBL PMC in a time-accurate simulation is orders of magnitude more computationally expensive. Consideration of various radiation models and TRI has significant effects on NO production, with orders of magnitude decrease in NO production observed as radiation is considered in combustion calculations.

Acknowledgments

This research was primarily supported by the National Aeronautics and Space Administration (NASA) under the research Grant # NNX07AB40A. The *P-3* approach presented here was developed by the senior author (mfm) while at the University of Karlsruhe, Germany in the framework of a Humboldt Research Award. The authors acknowledge the support provided by NASA, University of Karlsruhe and Alexander von Humboldt Foundation. The authors also like to thank the High Performance Computing Group of the University of California, San Diego for providing access to Triton, a high performance computational cluster.

References

[1] H. Pitsch, E. Riesmeier, N. Peters, Combust. Sci. Technol. 158 (2000) 389–406.
[2] R.S. Barlow, <http://www.ca.sandia.gov/TNF/> (accessed on 1.06.05).
[3] X.L. Zhu, J.P. Gore, A.N. Karpetis, R.S. Barlow, Combust. Flame 129 (2002) 342–345.
[4] G. Li, M.F. Modest, ASME J. Heat Transfer 125 (2003) 831–838.
[5] L. Wang, D.C. Haworth, S.R. Turns, M.F. Modest, Combust. Flame 141 (2005) 170–179.
[6] L. Wang, M.F. Modest, D.C. Haworth, S.R. Turns, Combust. Theory Model. 9 (2005) 479–498.
[7] M.F. Modest, ASME J. Heat Transfer 113 (1991) 650–656.
[8] M.K. Denison, B.W. Webb, ASME J. Heat Transfer 117 (1995) 359–365.
[9] M.F. Modest, H. Zhang, ASME J. Heat Transfer 124 (2002) 30–38.
[10] H. Zhang, M.F. Modest, J. Quant. Spectrosc. Radiat. Transfer 73 (2002) 349–360.
[11] H. Zhang, M.F. Modest, ASME J. Heat Transfer 125 (2003) 454–461.
[12] G. Pal, M.F. Modest, L. Wang, ASME J. Heat Transfer 130 (2008) 082701-1–082701-8.
[13] G. Pal, M.F. Modest, Comput. Therm. Sci. 1 (2009) 137–158.
[14] G. Pal, M.F. Modest, ASME J. Heat Transfer 132 (2010) 023307-1–023307-9.
[15] G. Pal, A. Wang, M.F. Modest, in: Proceedings of ASME Summer Heat Transfer Conference, Paper HT2009-88245, 2010.
[16] M.F. Modest, Radiative Heat Transfer, second ed., Academic Press, New York, 2003.
[17] M.F. Modest, J. Yang, J. Quant. Spectrosc. Radiat. Transfer 109 (2008) 1641–1666.
[18] D.C. Haworth, Prog. Energy Combust. Sci. 36 (2010) 168–259.
[19] G. Li, M.F. Modest, J. Quant. Spectrosc. Radiat. Transfer 73 (2002) 461–472.
[20] S.B. Pope, Prog. Energy Combust. Sci. 11 (1985) 119–192.
[21] V.P. Kabashnikov, G.I. Myasnikova, Heat Transfer Sov. Res. 17 (1985) 116–125.
[22] A. Wang, M.F. Modest, ASME J. Heat Transfer 128 (2006) 1041–1049.
[23] OpenFoam Website, <http://www.opencfd.co.uk/openfoam/>.
[24] A. Wang, M.F. Modest, D.C. Haworth, L. Wang, J. Quant. Spectrosc. Radiat. Transfer 109 (2008) 269–279.
[25] Y.Z. Zhang, D.C. Haworth, J. Comput. Phys. 194 (2004) 156–193.
[26] A. Wang, Investigation of turbulence–radiation interactions in turbulent flames using a hybrid FVM/particle-photon monte carlo approach (Ph.D. thesis), The Pennsylvania State University, University Park, PA, 2007.
[27] Q. Tang, J. Xu, S.B. Pope, Proc. Combust. Inst. 28 (2000) 133–139.
[28] R.S. Barlow, J.H. Frank, Proc. Combust. Inst. 27 (1998) 1087–1095.
[29] S. Mazumder, Numerical study of chemically reactive turbulent flows with radiative heat transfer (Ph.D. thesis), The Pennsylvania State University, University Park, PA, 1997.